# Supporting Information

## Wurm et al. 10.1073/pnas.1107553108

### SI Materials and Methods

**Western Blots.** Whole-cell protein extracts were prepared from cells grown to a confluence of ~80%. The cells were scratched from the surface of the cell-culture dish and boiled in SDS/PAGE sample buffer. The samples were analyzed by Western blotting using antibodies against Tom20, Tom22, and β-actin (Sigma–Aldrich).

**Preparation of Tom20 cDNAs.** The mRNAs of HeLa, Vero, and PtK2 cells were prepared using the GenElute mRNA Miniprep kit (Sigma-Aldrich). After reverse transcription using the ProtoScript AMV First-Strand cDNA Synthesis kit (New England Biolabs), sequencing was performed using primers against the first and last 20 nucleotides. The translated sequences were compared using the National Center for Biotechnology Information (NCBI) BLAST algorithm.

**Amino Acid Sequence Alignment of TOM Complex Subunits.** Amino acid sequences from various vertebrates (*Homo sapiens*, *Bos taurus*, *Rattus norvegicus*, *Mus musculus*, *Xenopus tropicalis*, and *Danio rerio*) were retrieved from Uniprot (Swissprot) and NCBI GenBank databases and were analyzed using the multiple alignment program ClustalW (1) using the default parameters. From these alignments, sequence identity matrices were prepared using the software BioEdit (2).

**Determining Physiological Parameters.** To evaluate the mitochondrial membrane potential, cells were grown on coverslips overnight and then were incubated for 20 min in growth medium containing 17.5 nM $DiOC_6$. After destaining in growth medium, living cells were mounted and imaged microscopically. To determine the respiratory rates, the cells were cultivated to a density of ~80% confluence, trypsinized, and resuspended in fresh growth medium. Then the oxygen consumption of the cells was measured for up to 20 min at room temperature using an oxygraph system (Hansatech Instruments). To determine the cellular growth rates, cells growing in culture flasks were trypsinized at different time-points and counted microscopically. For the analysis of the cytochrome *c* oxidase (COX) activity, a cytochemical staining procedure was used as described previously (3). In brief, cells were grown on coverslips, fixed, and incubated in 3,3-diaminobenzindine (DAB) staining solution. COX oxidizes DAB, which in turn polymerizes and precipitates. The amount of precipitate correlates to the COX activity.

**Stimulated Emission Depletion Microscopy.** For stimulated emission depletion (STED) microscopy and the corresponding confocal microscopy, a custom-built STED microscope was used. The fluorophore ATTO647N or KK114 was excited with a pulsed diode laser emitting 70-ps pulses at 635 nm (PicoQuant). STED was performed using a mode-locked titanium sapphire laser (MIRA900; Coherent) operating at 760 nm with a repetition rate of 76 MHz. The delay between the excitation and STED pulses was adjusted electronically. The STED beam was converted into a doughnut shape by passing the light through a polymeric phase plate (vortex pattern; RPC Photonics) and subsequently was overlaid with the excitation beam. The excitation and the STED beams were focused by a 100× oil immersion objective (NA 1.4 PL APO, 100×; Leica Microsystems). The fluorescence signal was collected by the same objective and detected confocally between 650 and 690 nm. The fluorescence was directed onto four counting avalanche photodiodes (SPCM-AQRH13; Perkin-Elmer) to avoid saturation effects caused by high photon fluxes. The images were obtained either by scanning the samples with a piezo stage (Nanoblock; Melles Griot) or by beam scanning (Yanus IV; TILL Photonics). Using this microscope, a resolution of ~250 nm in the confocal images and 40–50 nm in the STED images was achieved. Except for contrast stretching and smoothing, no further image processing was applied.

**Estimation of Cluster Sizes by Autocorrelation.** In image processing, 2D autocorrelations are used to evaluate the size of common features in an image (4). Here, autocorrelation was used to evaluate the size of protein clusters within mitochondria. The most prominent features within the images are the mitochondria themselves. To restrict the autocorrelation analysis to features within the mitochondria, squared regions of interest (ROIs) were cropped out and analyzed. To this end, images first were segmented to separate mitochondria from background using a binary mask created by smoothing, thresholding, and binarization. The skeleton (middle line) of the mitochondria was determined automatically and used for positioning the centers of the ROIs. Next, wherever possible, rectangular ROIs with an edge length of 260 nm (corresponding to 13 pixels on edge) completely covered by the mitochondria were selected and cropped out. Generally, up to 70 ROIs per image were selected and used for autocorrelation. To determine the size of common features in each square, a radial intensity distribution from the center of the autocorrelation image was calculated and plotted. Then, an exponential function was fit to the data for each ROI. The average size of the features in the image was deduced from the fitted curves. Note: The shapes of the clusters are not taken into account in this analysis. Finally, median values characterizing the size of the clusters were calculated on all obtained ROIs.

**Quantification of the Distribution of Tom20 Clusters.** Two algorithms were devised that allow the quantification of the distribution of Tom20 clusters: (*i*) an algorithm that identifies individual clusters within mitochondria and calculates their densities, and (*ii*) an algorithm that calculates the variance of the fluorescence intensity within the mitochondria.

**Image Segmentation.** Both algorithms require an automated identification of the mitochondrial interior. To this end, masks were created covering the mitochondrial interior.

These masks were generated in several steps. First, a simplified Anscombe transformation was applied to the raw images to compensate for inhomogeneities in the absolute intensity values. Then, to flatten large-scale inhomogeneities of fluorescence intensities while preserving intermediate and small-scale features (such as mitochondria and submitochondrial protein clusters), the equalized data were smoothed with a Gaussian function of 2 μm FWHM. The smoothed images were subtracted from the raw images, and negative intensity values were set to zero. To create a binary mask, enabling the separation of mitochondria from background, the difference image was binarized using a (local) isodata threshold. Next, the skeleton of the mitochondria was identified and enlarged to a diameter of 150 nm. In the final step, this midline mask was used to select the fraction of the image that was used for further analysis.

**Direct Determination of the Densities of Tom20 Clusters.** To determine the densities of Tom20 clusters, raw images were deconvolved linearly (Wiener filtering) using a Gaussian function of 44 nm FWHM as a kernel. To enhance small-scale intensity differences further and to compensate for large and intermediate-

scale fluorescence fluctuations, smoothed images were prepared to generate difference images in the following step. A smoothed image that contains only large-scale variations was generated by application of a median filter (kernel size: 100 nm) on the deconvolved image. This smoothed image was subtracted from the deconvolved image, and negative intensity values were set to zero, leading to an image that emphasizes small-scale differences in intensity. To exclude border effects, only the inner parts of the mitochondria were analyzed. To this end, a midline mask (diameter: 160 nm) was created using the segmentation algorithm outlined above.

To reject background, an isodata threshold was applied to select the brightest regions in the mitochondria (i.e., the regions containing clusters), resulting in a delicate mask. Within these segmented regions, single clusters were identified as local maxima of the fluorescence intensity. In a final step, the density of protein clusters, i.e., the number of clusters per area, was determined. In this evaluation of the density, clusters that were close to the border of the mask were excluded by applying a smaller midline mask with a diameter of only 150 nm. This algorithm requires a good signal-to-noise ratio.

**Variance Analysis.** To exclude an influence of the image segmentation process on the determined variance values, the local variance in the fluorescence intensity of raw STED images was calculated before image segmentation. To this end, the variance was determined in round ROIs with a diameter of seven pixels (~140 nm). The resulting variance values were assigned to the central pixel of the analyzed ROI. To evaluate the results of the analysis independently from the absolute brightness of the structures, the individual variance values were normalized to the squared average fluorescence intensity of the respective ROI. The variance calculation was repeated using each pixel successively as an ROI center, leading to an image in which each pixel represents the local variance. Finally, the mitochondria-containing fraction of the image was selected by image segmentation using masks as described above. Then, the median of the variance within the mitochondria was determined.


1. Larkin MA, et al. (2007) Clustal W and Clustal X version 2.0. *Bioinformatics* 23: 2947–2948.
2. Hall TA (1999) BioEdit: A user-friendly biological sequence alignment. analysis program for Windows 95/98/NT. *Nucleic Acids Symposium Series* 41:95–98.
3. Posakony JW, England JM, Attardi G (1975) Morphological heterogeneity of HeLa cell mitochondria visualized by a modified diaminobenzidine staining technique. *J Cell Sci* 19:315–329.
4. Hwang J, Gheber LA, Margolis L, Edidin M (1998) Domains in cell plasma membranes investigated by near-field scanning optical microscopy. *Biophys J* 74:2184–2190.


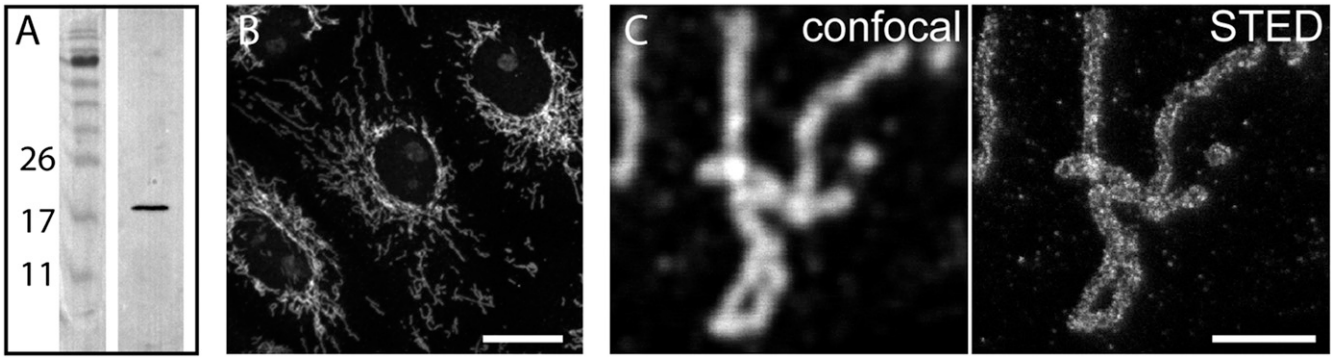


**Fig. S1.** Tom22 is localized in clusters in the mitochondrial outer membrane. (*A*) Western blot of a Vero cell extract decorated with the antiserum against Tom22. (*B*) Immunolabeling of Vero cells using the antiserum against Tom22. (Scale bar: 20 μm.) (*C*) STED microscopy (*Right*) reveals individual Tom22 clusters, which are blurred and not resolvable when using diffraction-limited confocal microscopy (*Left*). (Scale bar: 2 μm.).

Comparison of cDNA Sequences of Tom20 from HeLa, Vero and PtK2 cells:

```
HeLa   1   ATGGTGGGTCGGAACAGCGCCATCGCCGCCGGTGTATGCGGGGCCCTTTTCATTGGGTAC  60
Vero   1   ATGGTGGGTCGGAACAGCGCCATCGCCGCCGGTGTATGCGGAGCCCTTTTTATTGGGTAC  60
PtK2   1   ATGGTGGGTCGGAACAGCGCCATCGCCGCCGGCGTGTGCGGGGCCCTCTTCATCGGCTAC  60

HeLa   61  TGCATCTACTTCGACCGCAAAAGACGAAGTGACCCCAACTTCAAGAACAGGCTTCGAGAA  120
Vero   61  TGCATCTACTTCGATCGCAAAAGACGAAGTGACCCCAACTTCAAGAACAGGCTTCGAGAA  120
PtK2   61  TGTATTTACTTCGACCGCAAGAGACGGATGACCCCCAACTTCAAGAACAGGCTCCGAGTG  120

HeLa   121 CGAAGAAAGAAACAGAAGCTTGCCAAGGAGAGAGCTGGGCTTTCCAAGTTACCTGACCTT  180
Vero   121 CGAAGAAAGAAACAGAAGCTTGCCAAGGAGAGAGCTGGGCTTTCCAAGTTACCTGACCTT  180
PtK2   121 CGAAGAAAGAAACAGAAGCTTGCTAAAGAGAGAGCTGGGCTTTCCAAGTTACCGGACCTT  180

HeLa   181 AAAGATGCTGAAGCTGTTCAGAAGTTCTTCCTTGAAGAAATACAGCTTGGTGAAGAGTTA  240
Vero   181 AAAGATGCCGAAGCTGTTCAGAAGTTCTTTCTTGAAGAAATACAGCTTGGTGAGGAGTTA  240
PtK2   181 AAAGATGCAGAAGCTGTTCAGAAGTTCTTTCTTGAAGAAATACAACTTGGTGAGGAATTA  240

HeLa   241 CTAGCTCAAGGTGAATATGAGAAGGGCGTAGACCATCTGACAAATGCAATTGCTGTGTGT  300
Vero   241 CTAGCTCAAGGTGAATATGAGAAGGGCGTAGACCATCTGACAAATGCAATTGCTGTGTGT  300
PtK2   241 CTAGCCCAAGGCGAATATGAAAAAGGTGTCGACCACTGATCAAATGCCATTGCTGTCTGT  300

HeLa   301 GGACAGCCACAGCAGTTACTGCAGGTCTTACAGCAAACTCTTCCACCACCAGTGTTCCAG  360
Vero   301 GGACAGCCACAGCAGTTACTGCAGGTCTTACAGCAAACTCTTCCACCACCAGTGTTCCAA  360
PtK2   301 GGGCAACCACAGCAGTTGTTGCAAGTTTTACAGCAAACTCTTCCATCACCAGTGTTCCAA  360

HeLa   361 ATGCTTCTGACTAAGCTCCCAACAATTAGTCAGAGAATTGTAAGTGCTCAGAGCTTGGCT  420
Vero   361 ATGCTTCTGACTAAGCTCCCAACAATTAGTCAGAGAATTGTAAGTGCTCAGAGCTTGGCT  420
PtK2   361 ATGCTTCTGACTAAGCTACCAACAATTAGCCAGAGAATTGTGAGTGTCAGAAGCTTGGCT  420

HeLa   421 GAAGATGATGTGGAA      438
Vero   421 GAAGATGATGTGGAA      438
PtK2   421 GAAGATGATGTGGAA      438
```

**Fig. S2.** Comparison of the cDNA sequences of Tom20 from HeLa, Vero, and PtK2 cells. Differing bases are highlighted in yellow. The first and last 20 nucleotides of the respective sequences (shown in bold) were taken from the published human Tom20 cDNA sequence to generate primers and are thus not part of the authentic sequence.

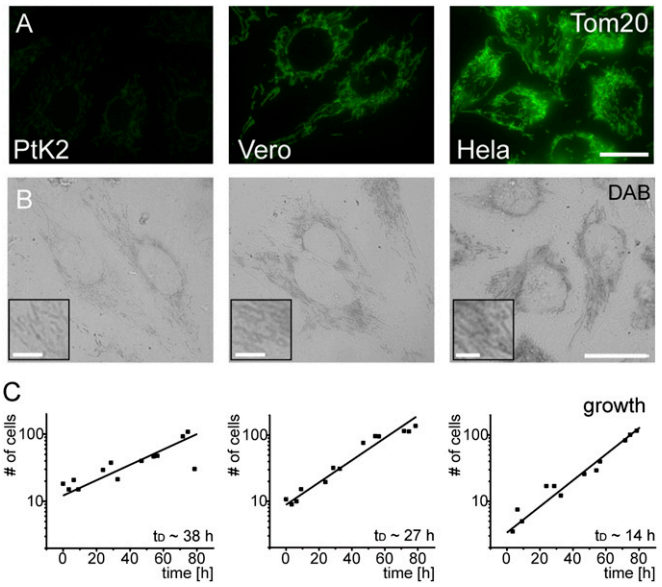


**Fig. S3.** Comparison of the three cell lines. (*A*) Fluorescence images of PtK2, Vero, and HeLa cells immunolabeled using the antiserum against Tom20. The same imaging conditions and color tables were used in the three cell lines to facilitate a comparison of the signal intensities. (Scale bar, 20 μm.) (*B*) Activity of the cytochrome *c* oxidase. The amount of DAB precipitate reflects the activity of the oxidase. (Scale bar: 30 μm.) (*Insets*) Magnification of the perinuclear region. (Scale bars: 4 μm.) (*C*) Growth rates. $t_D$, doubling time.

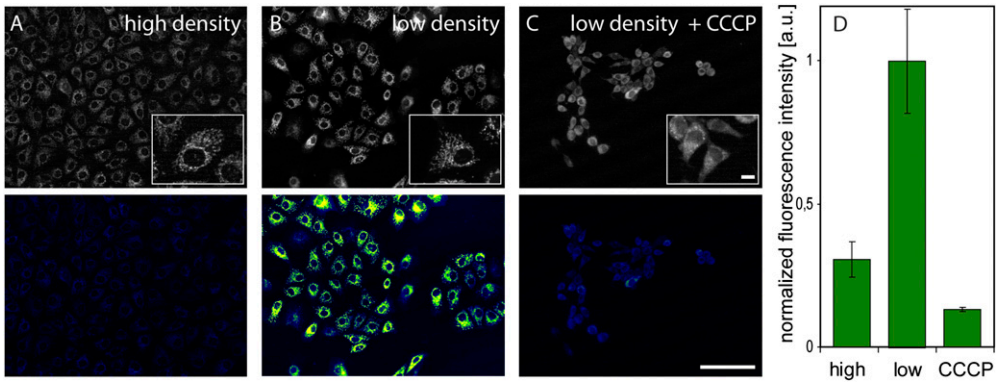


**Fig. S4.** Quantification of the $DiOC_6$ fluorescence signal in different growth conditions. PtK2 cells were grown to high (*A*) or low (*B* and *C*) density and incubated with $DiOC_6$. (*C*) Before $DiOC_6$ staining, cells were incubated for 10 h with 100 μM of the mitochondrial uncoupler carbonyl cyanide 3-chlorophenylhydrazone (CCCP). (*A–C*, *Upper*) Images of $DiOC_6$ fluorescence. The color tables were adjusted individually to provide an optimal signal-to-background ratio for each image. *Insets* show magnifications of the respective images. (*A–C*, *Lower*) Images of $DiOC_6$ fluorescence. Images shown are the same as in the upper row. Here, the same color table was used for the three images to enable comparison of the relative fluorescence intensities. (Scale bar: 100 μm; 10 μm in *Inset*) (*D*) Quantification of the respective mean fluorescence intensities. $n > 35$ images; each image included at least 20 cells. Error bars indicate SE.

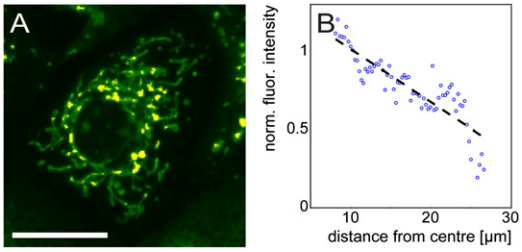


**Fig. S5.** Normalized distribution of $DiOC_6$ fluorescence intensity. (*A*) $DiOC_6$ labeling of a representative PtK2 cell. The same cell expressed matrix-targeted DsRed as a mitochondrial marker. (Scale bar: 20 μm.) (*B*) Plot of the $DiOC_6$ fluorescence intensities from the center to the rim of the single cell shown in *A* normalized with the DsRed signal of the same cell. Blue circles represent bins that pool the fluorescence intensity values. The dashed black line represents the linear fit to the binned fluorescence intensity values.

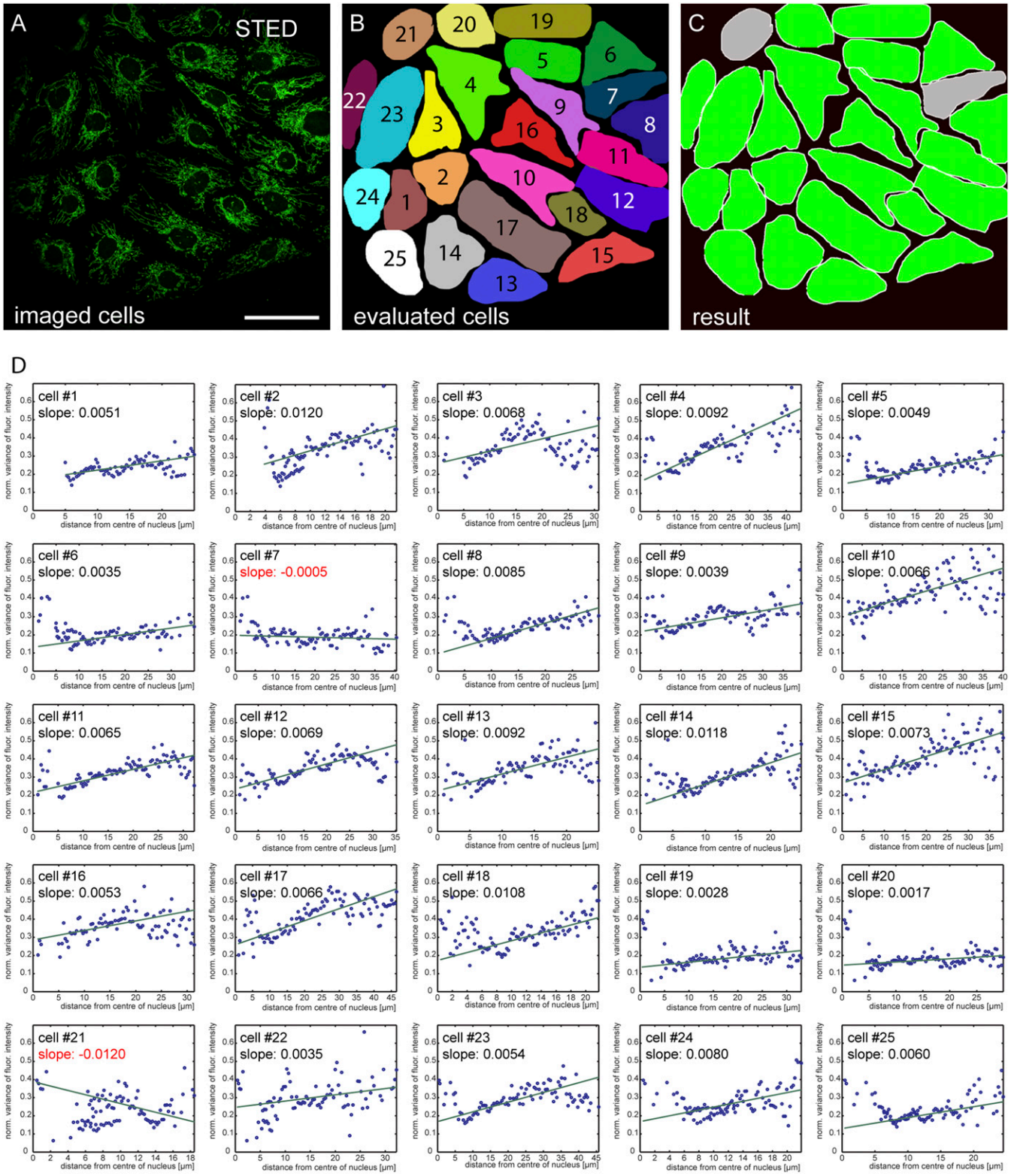


**Fig. S6.** Inner-cellular gradients of the normalized local variance of the Tom20 fluorescence signal. (*A*) STED image of a microcolony labeled with an antiserum against Tom20. (Scale bar: 50 µm.) (*B*) Graphical representation of all cells of the microcolony shown in *A*. (*C*) Green indicates cells in which the variance of the fluorescence signal is lower in the perinuclear mitochondria. In these cells the linear fits to the variance values have a positive slope. Gray indicates cells in which the linear fits have negative slopes. (*D*) Plots of the normalized mean variance values of the fluorescence signals radiating from the center of the respective cells to their borders. Cell numbers correspond to the numbering in *B*. Blue circles represent 100 bins that pool individual variance values. Black lines represent linear fits based on the individual variance values. A positive slope of the curve indicates that the density of the Tom20 clusters is higher in mitochondria around the nucleus than in mitochondria at the rim.

**Table S1. Amino acid sequence comparison of selected TOM-complex subunits of certain vertebrates**

| TOM complex subunit | *Homo sapiens* | *Bos taurus* | *Rattus norvegicus* | *Mus musculus* | *Xenopus tropicalis* | *Danio rerio* |
|---|---|---|---|---|---|---|
| Tom20 | | | | | | |
| *H. sapiens* | ID | 1 | 0.993 | 0.993 | 0.877 | 0.863 |
| *B. taurus* | | ID | 0.993 | 0.993 | 0.877 | 0.863 |
| *R. norvegicus* | | | ID | 1 | 0.884 | 0.869 |
| *M. musculus* | | | | ID | 0.884 | 0.869 |
| *X. tropicalis* | | | | | ID | 0.802 |
| *D. rerio* | | | | | | ID |
| Tom22 | | | | | | |
| *H. sapiens* | ID | 0.936 | 0.936 | 0.943 | 0.647 | 0.601 |
| *B. taurus* | | ID | 0.887 | 0.894 | 0.657 | 0.602 |
| *R. norvegicus* | | | ID | 0.978 | 0.633 | 0.594 |
| *M. musculus* | | | | ID | 0.64 | 0.601 |
| *X. tropicalis* | | | | | ID | 0.61 |
| *D. rerio* | | | | | | ID |
| Tom40 | | | | | | |
| *H. sapiens* | ID | 0.966 | 0.916 | 0.93 | 0.79 | 0.713 |
| *B. taurus* | | ID | 0.922 | 0.927 | 0.784 | 0.707 |
| *R. norvegicus* | | | ID | 0.983 | 0.754 | 0.683 |
| *M. musculus* | | | | ID | 0.759 | 0.688 |
| *X. tropicalis* | | | | | ID | 0.752 |
| *D. rerio* | | | | | | ID |
| Tom70 | | | | | | |
| *H. sapiens* | ID | 0.962 | 0.923 | 0.926 | 0.8 | 0.791 |
| *B. taurus* | | ID | 0.918 | 0.923 | 0.798 | 0.794 |
| *R. norvegicus* | | | ID | 0.983 | 0.776 | 0.773 |
| *M. musculus* | | | | ID | 0.774 | 0.769 |
| *X. tropicalis* | | | | | ID | 0.815 |
| *D. rerio* | | | | | | ID |

Compared are the respective homologous proteins in the different species. Results of sequence alignment showing the percentage of identical residues (1 = 100%) in the analyzed sequences. ID, identical sequences.

**Table S2. Entry numbers from Uniprot (Swissprot) and NCBI GenBank databases of sequences used for the analysis shown in Table S1**

| Species | Tom20 | Tom22 | Tom40 | Tom70 |
|---|---|---|---|---|
| *H. sapiens* | Q15388 | Q9NS69 | O96008 | O94826 |
| *B. taurus* | A6H7B1 | A6QPI6 | Q1LZB5 | Q08E34 |
| *R. norvegicus* | Q62760 | Q75Q41 | Q75Q40 | Q75Q39 |
| *M. musculus* | Q9DCC8 | Q9CPQ3 | Q9QYA2 | Q9CZW5 |
| *X. tropicalis* | Q6DFM9 | Q28BJ9 | Q6P825 | NP_001096527.1 |
| *D. rerio* | Q6DH66 | Q6IQJ1 | NP_955908.1 | AAH59538.1 |